

---

# FAST AND ACCURATE HIGH-ORDER METHOD FOR HIGH DIMENSIONAL SPACE-FRACTIONAL REACTION-DIFFUSION EQUATION WITH GENERAL BOUNDARY CONDITIONS

---

A PREPRINT

**Almushaira Mustafa**

School of Mathematics and Statistics  
Huazhong University of Science and Technology  
Wuhan 430074, China  
Department of Mathematics  
Sana'a University  
Sana'a, Yemen  
mstf1985@hust.edu.cn

**Harish Bhatt**

Department of Mathematics  
Center for Student Success & Retention  
Savannah State University  
Savannah, GA 31404  
bhatth@savannahstate.edu

February 28, 2022

## ABSTRACT

To achieve efficient and accurate long-time integration, we propose a fast, accurate, and stable high-order numerical method for solving fractional-in-space reaction-diffusion equations. The proposed method is explicit in nature and utilize the fourth-order compact finite difference scheme and matrix transfer technique (MTT) in space with FFT-based implementation. A time integration is done through the accurate fourth-order modified exponential time differencing Runge-Kutta scheme. The linear stability analysis and various numerical experiments including two-dimensional (2D) Fitzhugh-Nagumo, Gierer-Meinhardt, Gray-Scott and three-dimensional (3D) Schnakenberg models are presented to demonstrate the accuracy, efficiency and stability of the proposed method.

**Keywords** Space-fractional reaction-diffusion; Discrete fast transform; Matrix transfer technique; Exponential time differencing

## 1 Introduction

In this paper, a space-fractional reaction-diffusion equation (SFRDE) of the following form is considered:

$$\begin{cases} \frac{\partial u(\mathbf{x}, t)}{\partial t} = -\kappa(-\Delta)^{\alpha/2}u(\mathbf{x}, t) + f(u(\mathbf{x}, t), t), & (\mathbf{x}, t) \in \Omega \times (0, T], \ 1 < \alpha \leq 2, \\ u(\mathbf{x}, 0) = g(\mathbf{x}), & \mathbf{x} \in \Omega, \end{cases} \quad (1)$$

where  $\Omega$  is an open bounded domain in  $\mathbb{R}^d$ , ( $d = 1, 2, 3$ ),  $\kappa$  represents the diffusion coefficient,  $(-\Delta)^{\alpha/2}$  is the fractional Laplacian of order  $\alpha$  [18, 30, 26, 7, 25] defined through the eigenfunction expansion on a finite domain (see Definition 1) and  $f(u)$  is a nonlinear reaction term. The SFRDE (1) is provided with an initial condition  $g(\mathbf{x})$  and general boundary conditions such as periodic, homogeneous Dirichlet or Neumann boundary conditions.

Most numerical schemes for solving space-fractional diffusion problems involve applying the finite difference, finite volume, finite element, spectral method and so on for discretizing the fractional operator. Here, we focus our attention on matrix transfer technique (MTT) introduced by Ilic et al. in [18, 19] to solve space-fractional diffusion equations. Ding and Zhang [8] presented fourth-order methods based on the MTT for solving Riesz space-fractional diffusion and advection-dispersion equations. Yang et al. [30] utilized the MTT to solve fractional partial differential equations (FPDEs) with Riesz space-fractional derivative (RSFD). A rational approximation to dense matrix obtained from the

MTT was proposed by Aceto and Novati in [1] and its integral representation is approximated with the Gauss Jacobi quadrature rule.

There are many existing definitions of the fractional Laplacian operator, for more details, the readers are referred to [23, 9]. It is important to choose an appropriate numerical method of approximation accor to which definition is intended. The basic idea of the MTT is to approximate the fractional Laplacian  $(-\Delta)^{\alpha/2}$  by the matrix representation  $A^{\alpha/2}$ , where  $A$  is a symmetric positive definite matrix obtained from the discretization of the standard Laplace operator subject to the given boundary conditions. The main advantage of this approach is that, it gives a full diagonal representation of the fractional operator, being able to efficiently implement regardless of the fractional power in the problem. An additional advantage is that the application to two and three spatial dimensions is essentially the same as the one dimensional problem.

In this work, we propose a fast, accurate and stable compact exponential time differencing Runge-Kutta method for solving the multi-dimensional SFRDE (1). We use a fourth-order compact finite difference method and MTT for the spatial discretization, yiel a diagonalization matrix system of ordinary differential equations (ODEs) whose solution can be explicitly expressed in term of the time integrator. The proposed method can deal with various boundary conditions and take advantage of FFT-based computations. All these techniques are coupled together to produce fast, accurate and stable numerical method.

The rest of the paper is organized as follows. In Section 2, we recall an important definition and lemma. In Section 3, we discuss 1D, 2D and 3D versions of the proposed spatial discretization method with separate discussions for different types of boundary conditions. The time discretization is introduced in Section 4 and its linear stability analysis is presented. Furthermore, the 3D algorithm of the proposed method is provided with periodic boundary conditions. Extensive numerical experiments with applications are reported in Section 5 in order to numerically demonstrate accuracy, efficiency and stability of the proposed method. Some conclusion remarks are made in Section 6.

## 2 Preliminaries

In this section, the following definition and lemma which will be useful throughout this paper are recalled.

**Definition 1** For  $n, m, l = 0, 1, \dots$ , let the Laplacian  $(-\Delta)$  has a complete set of orthogonal eigenfunction  $\psi_n$ ,  $\psi_{n,m}$ , or  $\psi_{n,m,l}$  corresponding to eigenvalues  $\lambda_n$ ,  $\lambda_{n,m}$ , or  $\lambda_{n,m,l}$ , respectively, on a bounded region  $\Omega$  with periodic, homogeneous Dirichlet or homogeneous Neumann boundary conditions, then  $(-\Delta)^{\alpha/2}$  is defined by

$$\begin{aligned} (-\Delta)^{\alpha/2}u &= \sum_{n=0}^{\infty} \hat{u}_n \lambda_n^{\alpha/2} \psi_n, & d=1, \\ (-\Delta)^{\alpha/2}u &= \sum_{n=0}^{\infty} \sum_{m=0}^{\infty} \hat{u}_{n,m} \lambda_{n,m}^{\alpha/2} \psi_{n,m}, & d=2, \\ (-\Delta)^{\alpha/2}u &= \sum_{n=0}^{\infty} \sum_{m=0}^{\infty} \sum_{l=0}^{\infty} \hat{u}_{n,m,l} \lambda_{n,m,l}^{\alpha/2} \psi_{n,m,l}, & d=3, \end{aligned}$$

in which  $u$  can be expressed as follows

$$\begin{aligned} u &= \sum_{n=0}^{\infty} \hat{u}_n \psi_n, \quad \text{such that} \quad \sum_{n=0}^{\infty} |\hat{u}_n|^2 |\lambda_n|^{\alpha} < \infty, & d=1, \\ u &= \sum_{n=0}^{\infty} \sum_{m=0}^{\infty} \hat{u}_{n,m} \psi_{n,m}, \quad \text{such that} \quad \sum_{n=0}^{\infty} \sum_{m=0}^{\infty} |\hat{u}_{n,m}|^2 |\lambda_{n,m}|^{\alpha} < \infty, & d=2, \\ u &= \sum_{n=0}^{\infty} \sum_{m=0}^{\infty} \sum_{l=0}^{\infty} \hat{u}_{n,m,l} \psi_{n,m,l}, \quad \text{such that} \quad \sum_{n=0}^{\infty} \sum_{m=0}^{\infty} \sum_{l=0}^{\infty} |\hat{u}_{n,m,l}|^2 |\lambda_{n,m,l}|^{\alpha} < \infty, & d=3. \end{aligned}$$

**Lemma 1 ([34])** Suppose  $A$  be a positive definite matrix, and  $A = P\Lambda P^{-1}$ , where  $P$  is an orthogonal matrix and  $\Lambda$  is a diagonal matrix with diagonal entries being the eigenvalues of  $A$ , then for arbitrary real  $\alpha$ ,  $A^{\alpha} = P\Lambda^{\alpha}P^{-1}$  may be uniquely determined by  $A$  and  $\alpha$ .

### 3 Matrix transfer technique

In this section, a fourth-order compact difference scheme for discretizing the fractional operator  $(-\Delta)^{\alpha/2}$  is introduced and derived a fast algorithm via FFT-based implementation.

By using MTT developed by Ding and Zhang in [8] for discretizing the fractional operator  $(-\Delta)^{\alpha/2}$  with a uniform mesh of step size  $h$  in each spatial direction we obtain

$$(-\Delta)^{\alpha/2}u \approx \mathcal{T}^{\alpha/2}u, \quad (2)$$

where  $\mathcal{T}^{\alpha/2}$  is constructed from the eigenvalues and eigenvectors of the matrix representation of the standard Laplacian  $\mathcal{T}$  based on given boundary conditions. That is, the matrix  $\mathcal{T}^{\alpha/2}$  will be represented in the following subsections need not be formed explicitly.

Here, we use a fourth-order compact difference scheme for the Laplace operator

$$-\Delta \approx -h^{-2}(1 + \frac{1}{12}\delta_x^2)^{-1}\delta_x^2 + \mathcal{O}(h^4) \quad (3)$$

where  $\delta_x^2$  is the second-order central difference operator.

#### 3.1 One-dimensional case

Let us consider the model (1) in an open domain in the one-dimensional space  $\Omega = \{x_a < x < x_b\}$ . We denote  $\{x_n\}_{n=0}^N$  as the uniform grid points and  $h = \frac{x_b - x_a}{N}$  as the mesh size. Let  $u_n = u_n(t) \approx u_n(x_n, t)$  for  $0 \leq n \leq N$  denotes the numerical solution. Denote the solution vector as  $\mathbf{u} = (u_0, \dots, u_N)^T$ .

##### 3.1.1 The case of periodic boundary condition

For the periodic boundary condition, the matrix representation of standard Laplacian based on a fourth-order compact difference discretization reads:

$$-\Delta u(x, t) = (A^{-1}B) \mathbf{u}$$

where  $A_{N \times N}$ ,  $B_{N \times N}$  are the tridiagonal matrices as follows

$$A = \begin{bmatrix} \frac{5}{6} & \frac{1}{12} & 0 & \cdots & 0 & \frac{1}{12} \\ \frac{1}{12} & \frac{5}{6} & \frac{1}{12} & 0 & \cdots & 0 \\ 0 & \frac{1}{12} & \frac{5}{6} & \frac{1}{12} & 0 & \cdots \\ \vdots & \ddots & \ddots & \ddots & & \vdots \\ \cdots & 0 & \frac{1}{12} & \frac{5}{6} & \frac{1}{12} & 0 \\ 0 & \cdots & 0 & \frac{1}{12} & \frac{5}{6} & \frac{1}{12} \\ \frac{1}{12} & 0 & \cdots & 0 & \frac{1}{12} & \frac{5}{6} \end{bmatrix}$$

$$B = h^{-2} \begin{bmatrix} 2 & -1 & 0 & \cdots & 0 & -1 \\ -1 & 2 & -1 & 0 & \cdots & 0 \\ 0 & -1 & 2 & -1 & 0 & \cdots \\ \vdots & \ddots & \ddots & \ddots & & \vdots \\ \cdots & 0 & -1 & 2 & -1 & 0 \\ 0 & \cdots & 0 & -1 & 2 & -1 \\ -1 & 0 & \cdots & 0 & -1 & 2 \end{bmatrix}$$

and

$$\mathbf{u} = (u_1, \dots, u_N)^T.$$

Now, if  $\mathcal{T} = A^{-1}B$  is a matrix representation of a differential operator  $-\Delta$ , then the matrix representation of the fractional operator  $(-\Delta)^{\alpha/2}$  can be given by  $\mathcal{T}^{\alpha/2}$ . Since the matrices  $A$  and  $B$  are symmetric positive definite, they can be diagonalized as [20, 33, 16, 17, 2]

$$\mathcal{T} = A^{-1}B = P\Lambda P^{-1} = (P\Lambda P^{-1})^T = P^{-1}\Lambda P, \quad (4)$$

where  $\Lambda$  is the diagonal eigenvalues matrix, that is,

$$\Lambda = \text{diag}(\lambda_1, \dots, \lambda_N), \quad \lambda_n = \frac{4 \sin^2(\frac{(n-1)\pi}{2N})}{h^2 \left(1 - \frac{1}{3} \sin^2(\frac{(n-1)\pi}{2N})\right)}, \quad 1 \leq n \leq N, \quad (5)$$

and  $P_{N \times N}$  is the eigenvectors matrix, that is,

$$P_{i,j} = \exp\left(\frac{-\sqrt{-1}(i-1)(j-1)2\pi}{N}\right), \quad i, j = 1, \dots, N. \quad (6)$$

Using the MTT, the matrix representation of fractional Laplacian reads

$$(-\Delta)^{\alpha/2} u(x, t) = \left(P^{-1} \Lambda^{\alpha/2} P\right) \mathbf{u}. \quad (7)$$

Substituting (7) into (1) yields the semi-discretization in space of the one-dimensional SFRDE:

$$\frac{\partial \mathbf{u}}{\partial t} = -\kappa \left(P^{-1} \Lambda^{\alpha/2} P\right) \mathbf{u} + \mathbf{f}(\mathbf{u}, t), \quad (8)$$

where  $\mathbf{f}(\mathbf{u}, t) = (f(u_1, t), \dots, f(u_N, t))^T$ . If  $N$  is large, the computational cost of the matrix-vector product in (7) is extremely high. Hence, we will propose a fast algorithm to efficiently compute matrix-vector product in (7). From the definition of  $P$  in (6), it is pointed out in [20] that the product  $P\mathbf{u}$  is equivalent to the Discrete Fourier transform (DFT) [27] of the vector  $\mathbf{u}$ , namely,  $P\mathbf{u} = \mathcal{F}(\mathbf{u})$ , ( $\mathcal{F}$  stands for DFT), while  $P^{-1}\mathbf{u}$  can be obtained via the inverse DFT of  $\mathbf{u}$ , that is,  $P^{-1}\mathbf{u} = \mathcal{F}^{-1}(\mathbf{u})$ .

Multiplying  $P$  from the left hand side in (8), we immediately obtain

$$\frac{\partial \mathcal{F}(\mathbf{u})}{\partial t} = -\kappa \Lambda^{\alpha/2} \mathcal{F}(\mathbf{u}) + \mathcal{F}(\mathbf{f}(\mathbf{u}, t)). \quad (9)$$

Thus, the computational complexity of evaluating the matrix-vector product in (7) can be reduced from  $\mathcal{O}(N^2)$  to  $\mathcal{O}(N \log(N))$ .

### 3.1.2 The case of homogenous Dirichlet boundary condition

For the homogenous Dirichlet boundary condition, the matrix representation of standard Laplacian reads as:

$$-\Delta u(x, t) = (A^{-1} B) \mathbf{u},$$

where  $A_{(N-1) \times (N-1)}$ ,  $B_{(N-1) \times (N-1)}$  are the tridiagonal matrices as follows

$$A = \begin{bmatrix} \frac{5}{6} & \frac{1}{12} & 0 & \cdots & 0 & 0 \\ \frac{1}{12} & \frac{5}{6} & \frac{1}{12} & 0 & \cdots & 0 \\ 0 & \frac{1}{12} & \frac{5}{6} & \frac{1}{12} & 0 & \cdots \\ \vdots & \ddots & \ddots & \ddots & & \vdots \\ \cdots & 0 & \frac{1}{12} & \frac{5}{6} & \frac{1}{12} & 0 \\ 0 & \cdots & 0 & \frac{1}{12} & \frac{5}{6} & \frac{1}{12} \\ 0 & 0 & \cdots & 0 & \frac{1}{12} & \frac{5}{6} \end{bmatrix}$$

$$B = h^{-2} \begin{bmatrix} 2 & -1 & 0 & \cdots & 0 & 0 \\ -1 & 2 & -1 & 0 & \cdots & 0 \\ 0 & -1 & 2 & -1 & 0 & \cdots \\ \vdots & \ddots & \ddots & \ddots & & \vdots \\ \cdots & 0 & -1 & 2 & -1 & 0 \\ 0 & \cdots & 0 & -1 & 2 & -1 \\ 0 & 0 & \cdots & 0 & -1 & 2 \end{bmatrix}$$

and

$$\mathbf{u} = (u_1, \dots, u_{N-1})^T.$$

Similarly, the matrix representation of fractional Laplacian reads:

$$(-\Delta)^{\alpha/2} u(x, t) = \left(P^{-1} \Lambda^{\alpha/2} P\right) \mathbf{u},$$

where

$$\Lambda = \text{diag}(\lambda_1, \dots, \lambda_{N-1}), \quad \lambda_n = \frac{4 \sin^2(\frac{n\pi}{2N})}{h^2 (1 - \frac{1}{3} \sin^2(\frac{n\pi}{2N}))}, \quad 1 \leq n \leq N-1, \quad (10)$$

and

$$P_{i,j} = \sin\left(\frac{ij\pi}{N}\right), \quad i, j = 1, \dots, N-1. \quad (11)$$

From the definition of  $P$  in (11), it is noted that the operations  $P\mathbf{u}$  and  $P^{-1}\mathbf{u}$  are exactly the Discrete Sine Transform (DST) and the inverse DST respectively, and can be efficiently evaluated by FFT-based algorithm [27].

### 3.1.3 The case of homogenous Neumann boundary condition

For the homogenous Neumann boundary condition, the matrix representation of standard Laplacian reads:

$$-\Delta u(x, t) = (A^{-1}B)\mathbf{u},$$

where  $A_{(N+1) \times (N+1)}$ ,  $B_{(N+1) \times (N+1)}$  are the tridiagonal matrices as follows

$$A = \begin{bmatrix} \frac{5}{6} & \frac{1}{6} & 0 & \dots & 0 & 0 \\ \frac{1}{12} & \frac{5}{6} & \frac{1}{12} & 0 & \dots & 0 \\ 0 & \frac{1}{12} & \frac{5}{6} & \frac{1}{12} & 0 & \dots \\ \vdots & \ddots & \ddots & \ddots & & \vdots \\ \dots & 0 & \frac{1}{12} & \frac{5}{6} & \frac{1}{12} & 0 \\ 0 & \dots & 0 & \frac{1}{12} & \frac{5}{6} & \frac{1}{12} \\ 0 & 0 & \dots & 0 & \frac{1}{6} & \frac{5}{6} \end{bmatrix}$$

$$B = h^{-2} \begin{bmatrix} 2 & -2 & 0 & \dots & 0 & 0 \\ -1 & 2 & -1 & 0 & \dots & 0 \\ 0 & -1 & 2 & -1 & 0 & \dots \\ \vdots & \ddots & \ddots & \ddots & & \vdots \\ \dots & 0 & -1 & 2 & -1 & 0 \\ 0 & \dots & 0 & -1 & 2 & -1 \\ 0 & 0 & \dots & 0 & -2 & 2 \end{bmatrix}$$

and

$$\mathbf{u} = (u_0, \dots, u_N)^T.$$

Similarly, the matrix representation of fractional Laplacian reads:

$$(-\Delta)^{\alpha/2} u(x, t) = (P^{-1} \Lambda^{\alpha/2} P)\mathbf{u},$$

where

$$\Lambda = \text{diag}(\lambda_1, \dots, \lambda_{N-1}), \quad \lambda_n = \frac{4 \sin^2(\frac{n\pi}{2N})}{h^2 (1 - \frac{1}{3} \sin^2(\frac{n\pi}{2N}))}, \quad 0 \leq n \leq N, \quad (12)$$

and

$$P_{i,j} = \cos\left(\frac{ij\pi}{N}\right), \quad i, j = 0, \dots, N. \quad (13)$$

In order to reduce the computational complexity of  $P\mathbf{u}$  or  $P^{-1}\mathbf{u}$  from  $\mathcal{O}(N^2)$  to  $\mathcal{O}(N \log(N))$  by a FFT-based fast algorithm, we follow the idea in [20]. To this end, let  $\mathbf{u} = (u_0, \dots, u_N)^T$  be any vector of size  $N+1$  and similarly define its reflection vector of size  $N+1$  as  $\mathbf{v} = (u_{N-1}, \dots, u_1)^T$ , and apply a DFT to  $(\mathbf{u}, \mathbf{v})^T$  and then take the first  $N+1$  components of the result which is equivalent to operation  $P\mathbf{u}$  and also apply an inverse DFT to  $(\mathbf{u}, \mathbf{v})^T$  and then take the first  $N+1$  components of the result which is equivalent to operation  $P^{-1}\mathbf{u}$ .

### 3.2 Two-dimensional case

For  $d = 2$ , we suppose  $\Omega = \{x_a < x < x_b, y_a < y < y_b\}$ . With loss of generality, we partition the spatial domain  $\Omega$  by a square grid which is uniform in each direction, i.e.,  $h = \frac{x_b - x_a}{N} = \frac{y_b - y_a}{N}$ . Mesh points are defined as  $(x_n, y_m) = (x_a + nh, y_a + mh)$  for  $n, m = 0, \dots, N$ . Let  $u_{n,m} = u_{n,m}(t)$  represent the numerical approximation of the solution  $u(x_n, y_m, t)$ , for  $n, m = 0, \dots, N$ . Denote the 2D solution array as  $U = \{u_{n,m}\}_{(N+1, N+1)}$ .

For the periodic boundary condition, following the same arguments of the one-dimensional case, the discretization of fractional Laplacian can be expressed as:

$$(-\Delta)^{\alpha/2} u(x, y, t) = \left( \mathcal{T}_x^{\alpha/2} U + U (\mathcal{T}_y^{\alpha/2})^T \right), \quad (14)$$

where the matrices  $\mathcal{T}_x = A^{-1}B$  and  $\mathcal{T}_y = A^{-1}B$  are given in (4). Define the special operators  $\otimes$  and  $\odot$  as follows  $\mathcal{T}_x \otimes U = \mathcal{T}_x U$  and  $\mathcal{T}_y \odot U = U \mathcal{T}_y^T$ , that is

$$(\mathcal{T}_x \otimes U)_{n,m} = \sum_{k=1}^N (\mathcal{T}_x)_{n,k} u_{k,m}, \quad (\mathcal{T}_y \odot U)_{n,m} = \sum_{k=1}^N (\mathcal{T}_y)_{n,k} u_{n,k}.$$

Note that these two operators are commutative, i.e.,  $\mathcal{T}_x \otimes \mathcal{T}_y \odot U = \mathcal{T}_y \odot \mathcal{T}_x \otimes U$ . Then we can rewrite (14) in the following compact representation

$$(-\Delta)^{\alpha/2} u(x, y, t) = h^{-\alpha} \left( \mathcal{T}_x^{\alpha/2} \otimes U + \mathcal{T}_y^{\alpha/2} \odot U \right). \quad (15)$$

Define another operator  $\odot$  for element by element multiplication two arrays of same sizes as

$$(A \odot B)_{i,j} = (B \odot A)_{i,j} = A_{i,j} B_{i,j}.$$

Then, the fractional Laplacian can be reformulated as

$$(-\Delta)^{\alpha/2} u(x, y, t) = P_y^{-1} \odot P_x^{-1} \otimes \left( \Lambda^{\alpha/2} \odot (P_y \odot P_x \otimes U) \right), \quad (16)$$

where  $\Lambda_{n,m} = h^{-2} \left( \frac{4 \sin^2(\frac{(n-1)\pi}{2N})}{1 - \frac{1}{3} \sin^2(\frac{(n-1)\pi}{2N})} + \frac{4 \sin^2(\frac{(m-1)\pi}{2N})}{1 - \frac{1}{3} \sin^2(\frac{(m-1)\pi}{2N})} \right)$ , for  $n, m = 1, \dots, N$ ,  $P_x$  and  $P_y$  are orthogonal matrices be given in (6) and  $U = \{u_{n,m}\}_{(N,N)}$ .

For the homogenous Dirichlet boundary condition, the fractional Laplacian can be similarly expressed as:

$$(-\Delta)^{\alpha/2} u(x, y, t) = P_y^{-1} \odot P_x^{-1} \otimes \left( \Lambda^{\alpha/2} \odot (P_y \odot P_x \otimes U) \right), \quad (17)$$

where  $\Lambda_{n,m} = h^{-2} \left( \frac{4 \sin^2(\frac{n\pi}{2N})}{1 - \frac{1}{3} \sin^2(\frac{n\pi}{2N})} + \frac{4 \sin^2(\frac{m\pi}{2N})}{1 - \frac{1}{3} \sin^2(\frac{m\pi}{2N})} \right)$ , for  $n, m = 1, \dots, N-1$ ,  $P_x$  and  $P_y$  are orthogonal matrices be given in (11) and  $U = \{u_{n,m}\}_{(N-1, N-1)}$ .

For the homogenous Neumann boundary condition, the fractional Laplacian can be similarly expressed as:

$$(-\Delta)^{\alpha/2} u(x, y, t) = P_y^{-1} \odot P_x^{-1} \otimes \left( \Lambda^{\alpha/2} \odot (P_y \odot P_x \otimes U) \right), \quad (18)$$

where  $\Lambda_{n,m} = h^{-2} \left( \frac{4 \sin^2(\frac{n\pi}{2N})}{1 - \frac{1}{3} \sin^2(\frac{n\pi}{2N})} + \frac{4 \sin^2(\frac{m\pi}{2N})}{1 - \frac{1}{3} \sin^2(\frac{m\pi}{2N})} \right)$ , for  $n, m = 0, \dots, N$ ,  $P_x$  and  $P_y$  are orthogonal matrices be given in (13) and  $U = \{u_{n,m}\}_{(N+1, N+1)}$ .

Plugging the above equations (16), (17) or (18) into (1) and multiplying  $P_x$  from the left hand side and  $P_y^T$  from the right hand side, we obtain the semi-discretization in space of the two-dimensional SFRDE:

$$\frac{\partial \mathcal{F}(U)}{\partial t} = -\kappa \Lambda^{\alpha/2} \mathcal{F}(U) + \mathcal{F}(f(U, t)), \quad (19)$$

where  $\mathcal{F}(U) = P_y \odot P_x \otimes U$  and  $\mathcal{F}(f(U, t)) = P_y \odot P_x \otimes f(U, t)$ .

We note that the operation  $P_y \odot P_x \otimes U$  can be deficiency computed by FFT-based computation, thus the computational complexity can be reduced from  $\mathcal{O}(N^3)$  to  $\mathcal{O}(N^2 \log(N))$ .

### 3.3 Three-dimensional case

For  $d = 3$ , let  $\Omega = \{x_a < x < x_b, y_a < y < y_b, z_a < z < z_b\}$ . For simplicity, we denote  $h$  as the spatial space and  $N$  as the number of grid intervals in each direction. Set  $u_{n,m,l} = u_{n,m,l}(t) \approx u(x_n, y_m, z_l, t)$  for  $n, m, l = 0, \dots, N$ . Denote the unknowns as a three-dimensional array  $U = \{u_{n,m,l}\}_{(N+1, N+1, N+1)}$ . With similar process, we can write the fractional Laplacian as the following compact representation

$$(-\Delta)^{\alpha/2} u(x, y, z, t) = \left( \mathcal{T}_x^{\alpha/2} \otimes U + \mathcal{T}_y^{\alpha/2} \otimes U + \mathcal{T}_z^{\alpha/2} \otimes U \right), \quad (20)$$

where the spacial operator are redefined as

$$(\mathcal{T}_x \otimes U)_{n,m,l} = \sum_{k=0}^N (\mathcal{T}_x)_{n,k} u_{k,m,l}, \quad (\mathcal{T}_y \otimes U)_{n,m,l} = \sum_{k=0}^N (\mathcal{T}_y)_{m,k} u_{n,k,l}, \quad (\mathcal{T}_z \otimes U)_{n,m,l} = \sum_{k=0}^N (\mathcal{T}_z)_{l,k} u_{n,m,k}.$$

Following the similar analysis in two dimensional case, the fractional Laplacian can be reformulated as follows

$$(-\Delta)^{\alpha/2} u(x, y, z, t) = P_z^{-1} \otimes P_y^{-1} \otimes P_x^{-1} \otimes \left( \Lambda^{\alpha/2} \odot (P_z \otimes P_y \otimes P_x \otimes U) \right), \quad (21)$$

where

$$\Lambda_{n,m,l} = h^{-2} \left( \frac{4 \sin^2(\frac{(n-1)\pi}{2N})}{1 - \frac{1}{3} \sin^2(\frac{(n-1)\pi}{2N})} + \frac{4 \sin^2(\frac{(m-1)\pi}{2N})}{1 - \frac{1}{3} \sin^2(\frac{(m-1)\pi}{2N})} + \frac{4 \sin^2(\frac{(l-1)\pi}{2N})}{1 - \frac{1}{3} \sin^2(\frac{(l-1)\pi}{2N})} \right), \quad n, m, l = 1, \dots, N,$$

(in the case of periodic boundary conditions)

$$\Lambda_{n,m,l} = h^{-2} \left( \frac{4 \sin^2(\frac{n\pi}{2N})}{1 - \frac{1}{3} \sin^2(\frac{n\pi}{2N})} + \frac{4 \sin^2(\frac{m\pi}{2N})}{1 - \frac{1}{3} \sin^2(\frac{m\pi}{2N})} + \frac{4 \sin^2(\frac{l\pi}{2N})}{1 - \frac{1}{3} \sin^2(\frac{l\pi}{2N})} \right), \quad n, m, l = 1, \dots, N-1,$$

(in the case of homogenous Dirichlet boundary conditions)

$$\Lambda_{n,m,l} = h^{-2} \left( \frac{4 \sin^2(\frac{n\pi}{2N})}{1 - \frac{1}{3} \sin^2(\frac{n\pi}{2N})} + \frac{4 \sin^2(\frac{m\pi}{2N})}{1 - \frac{1}{3} \sin^2(\frac{m\pi}{2N})} + \frac{4 \sin^2(\frac{l\pi}{2N})}{1 - \frac{1}{3} \sin^2(\frac{l\pi}{2N})} \right), \quad n, m, l = 0, \dots, N,$$

(in the case of homogenous Neumann boundary conditions)

and  $P_x, P_y$  and  $P_z$  are orthogonal matrices be given in (6) for periodic boundary conditions, be defined in (11) for homogenous Dirichlet boundary conditions or be defined in (13) for homogenous Neumann boundary conditions.

The following is the semi-discretization in space of the three-dimensional SFRDE:

$$\frac{\partial \mathcal{F}(U)}{\partial t} = -\kappa \Lambda^{\alpha/2} \mathcal{F}(U) + \mathcal{F}(f(U, t)), \quad (22)$$

where  $\mathcal{F}(U) = P_z \otimes P_y \otimes P_x \otimes U$  and  $\mathcal{F}(f(U, t)) = P_z \otimes P_y \otimes P_x \otimes f(U, t)$ .

**Remark 1** The overall computational cost of the proposed method can be reduced from  $\mathcal{O}(N^{d+1})$  to  $\mathcal{O}(N^d \log(N))$  for  $d = 1, 2$ , or  $3$ , per time step by using FFT-based fast calculation.

## 4 Exponential time differencing procedure

Consider the following nonlinear initial boundary value problem

$$U_t + \mathcal{A}U = f(U, t), \quad U \in \Omega, t = (0, T], \quad (23)$$

where  $\mathcal{A}$  represents a spatial discretization of Laplacian operator. Let  $\tau$  be the temporal step size, then using a variation of constant formula, then the exact solution of (23) is the following recurrence formula

$$U(t_{k+1}) = e^{-\tau \mathcal{A}} U(t_k) + \tau \int_0^1 e^{-\tau \mathcal{A}(1-s)} f(U(t_k + s\tau), t_k + s\tau) ds. \quad (24)$$

The various exponential time differencing (ETD) methods come into picture from how one approximates the integral term. Here, we utilize a fourth-order time stepping scheme as considered by [4] which is based on fourth-order Padé

(1, 3) approximation to  $e^{-z}$ . The Padé approximations are known rational approximations. In particular, Padé (1, 3) approximation to  $e^{-z}$  is given by

$$R_{1,3}(z) = \frac{24 - 6z}{24 + 18z + 6z^2 + z^3}, \quad (25)$$

where the notation  $R_{1,3}(z)$  is used for Padé (1, 3) approximation to  $e^{-z}$ . Fig. 1 (left) shows the behavior of the exponential function  $e^{-z}$  and  $R_{1,3}(z)$  for  $z \in [0, 60]$ , while Fig. 1 (right) shows the behavior of the function  $R_{1,3}(z)$  for  $z = (x, y) \in [0, 20] \times [-10, 10]$ .

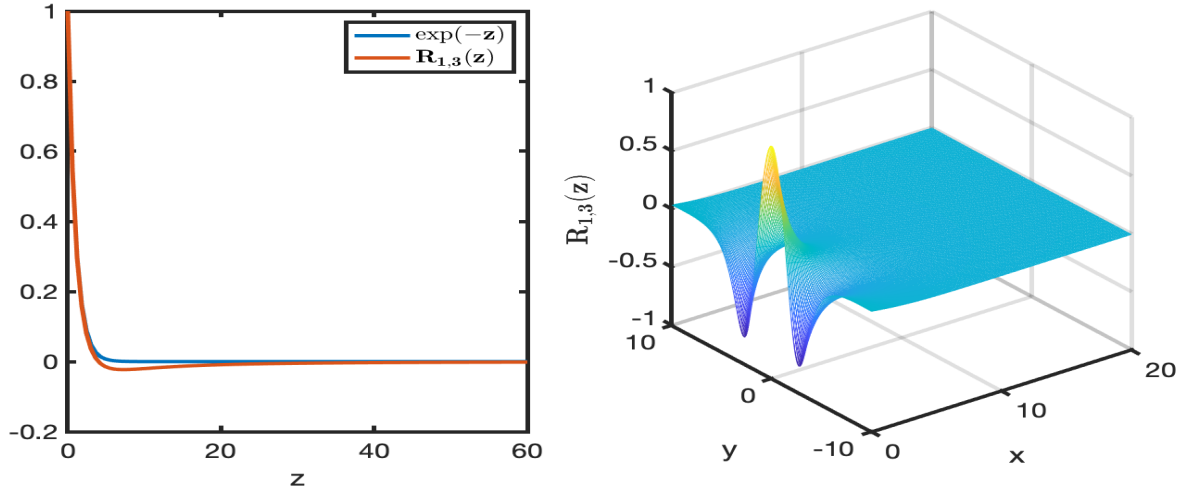


Figure 1: Left label: Behavior of the functions  $e^{-z}$  and  $R_{1,3}(z)$  for  $z \in [0, 60]$ . Right label: Behavior of the function  $R_{1,3}(z)$  approximation of  $e^{-z}$  for  $z = (x, y) \in [0, 20] \times [-10, 10]$ .

Following the process in [4], the ETDRK4-P13 method reads as:

$$\begin{aligned} U^{k+1} = & R_{1,3}(\tau\mathcal{A})U^k + \phi_1(\tau\mathcal{A})f(U^k, t_k) + \phi_2(\tau\mathcal{A}) (f(a^k, t_k + \tau/2) + f(b^k, t_k + \tau/2)) \\ & + \phi_3(\tau\mathcal{A})f(c^k, t_k + \tau), \end{aligned} \quad (26)$$

where

$$\begin{aligned} a^k &= R_{1,3}(\tau/2\mathcal{A})U^k + \phi(\tau/2\mathcal{A})f(U^k, t_k), \\ b^k &= R_{1,3}(\tau/2\mathcal{A})U^k + \phi(\tau/2\mathcal{A})f(a^k, t_k + \tau/2), \\ c^k &= R_{1,3}(\tau/2\mathcal{A})a^k + \phi(\tau/2\mathcal{A}) (2f(b^k, t_k + \tau/2) - f(u^k, t_k)), \end{aligned}$$

with

$$\begin{aligned} R_{1,3}(\tau\mathcal{A}) &= (24\mathcal{I} - 6\tau\mathcal{A}) (24\mathcal{I} + 18\tau\mathcal{A} + 6\tau^2\mathcal{A}^2 + \tau^3\mathcal{A}^3)^{-1}, \\ R_{1,3}(\tau/2\mathcal{A}) &= 24(8\mathcal{I} - \tau\mathcal{A}) (192\mathcal{I} + 72\tau\mathcal{A} + 12\tau^2\mathcal{A}^2 + \tau^3\mathcal{A}^3)^{-1}, \\ \phi_1(\tau\mathcal{A}) &= \tau(4\mathcal{I} - \tau\mathcal{A}) (24\mathcal{I} + 18\tau\mathcal{A} + 6\tau^2\mathcal{A}^2 + \tau^3\mathcal{A}^3)^{-1}, \\ \phi_2(\tau\mathcal{A}) &= 2\tau(4\mathcal{I} + \tau\mathcal{A}) (24\mathcal{I} + 18\tau\mathcal{A} + 6\tau^2\mathcal{A}^2 + \tau^3\mathcal{A}^3)^{-1}, \\ \phi_3(\tau\mathcal{A}) &= \tau(4\mathcal{I} + 3\tau\mathcal{A} + \tau^2\mathcal{A}^2) (24\mathcal{I} + 18\tau\mathcal{A} + 6\tau^2\mathcal{A}^2 + \tau^3\mathcal{A}^3)^{-1}, \\ \phi(\tau/2\mathcal{A}) &= \tau(96\mathcal{I} + 12\tau\mathcal{A} + \tau^2\mathcal{A}^2) (192\mathcal{I} + 72\tau\mathcal{A} + 12\tau^2\mathcal{A}^2 + \tau^3\mathcal{A}^3)^{-1}, \end{aligned}$$

where  $\mathcal{I}$  is an identity matrix.

#### 4.1 FFT implementation of ETDRK4-P13 method

For the efficient implementation of ETDRK4-P13, in the following algorithm the FFT computations of the ETDRK4-P13 method is provided for the case of 3D SFRD with periodic boundary conditions:



---

**Algorithm 1** ETD RK4-P13 Method

---

```

1: Given  $\Lambda^{\alpha/2}$ .
2: Set  $L = \kappa\tau\Lambda^{\alpha/2}$ .
3: Precompute the following 3D arrays:
4:  $R_{13} = (24\mathcal{I} - 6L)(24\mathcal{I} + 18L + 6L^2 + L^3)^{-1}$ .
5:  $Q_{13} = 24(8\mathcal{I} - L)(192\mathcal{I} + 72L + 12L^2 + L^3)^{-1}$ .
6:  $\phi = \tau(96\mathcal{I} + 12L + L^2)(192\mathcal{I} + 72L + 12L^2 + L^3)^{-1}$ .
7:  $\phi_1 = \tau(4\mathcal{I} - L)(24\mathcal{I} + 18L + 6L^2 + L^3)^{-1}$ .
8:  $\phi_2 = 2\tau(4\mathcal{I} + L)(24\mathcal{I} + 18L + 6L^2 + L^3)^{-1}$ .
9:  $\phi_3 = \tau(4\mathcal{I} + 3L + L^2)(24\mathcal{I} + 18L + 6L^2 + L^3)^{-1}$ .
10: for  $k = 0, 1, \dots, M - 1$  do
11:    $t_k = k\tau$ .
12:    $u_h = \text{fftn}(u)$ . ▷ MATLAB build-in function
13:   Compute  $f(u, t_k)$  as  $f_u$ .
14:    $a_k = \text{ifftn}(Q_{13} \odot u_h + \phi \odot \text{fftn}(f_u))$ . ▷ The operator  $\odot$  stands for element by element multiplication
15:   Compute  $f(a_k, t_k + \tau/2)$  as  $f_a$ .
16:    $b_k = \text{ifftn}(Q_{13} \odot u_h + \phi \odot \text{fftn}(f_a))$ .
17:   Compute  $f(b_k, t_k + \tau/2)$  as  $f_b$ .
18:    $c_k = \text{ifftn}(Q_{13} \odot \text{fftn}(a_k) + \phi \odot \text{fftn}(2f_b - f_u))$ .
19:   Compute  $f(c_k, t_k + \tau)$  as  $f_c$ .
20:    $u = \text{ifftn}(R_{13} \odot u_h + \phi_1 \odot \text{fftn}(f_u) + \phi_2 \odot \text{fftn}(f_a + f_b) + \phi_3 \odot \text{fftn}(f_c))$ .
21: end for

```

---

## 4.2 Linear analysis

The linear truncation error and stability analysis of the ETD RK4-P13 method (26) are performed in this subsection.

### 4.2.1 Truncation error of ETD RK4-P13

It is obvious that the overall spatial discretization is of order four because a fourth-order compact finite difference scheme is applied to fractional Laplacian term. Here, we analysis the overall local temporal truncation error for (26) scheme by using Taylor expansion. To this end, we consider the following linear semi-discretization system

$$\frac{\partial \mathbf{v}}{\partial t} + \mathcal{A}\mathbf{v} = \mathcal{B}\mathbf{v} \quad (27)$$

where  $\mathcal{A}$  and  $\mathcal{B}$  represent matrices derived from the linear spatial discretization of fractional Laplacian and reaction term of a linear space-fractional reaction-diffusion system respectively, and  $\mathbf{v}$  is a vector of unknowns.

Similar to the previous approach introduced in [32, 5], we apply (26) to the system (27) as follows

$$\mathbf{v}^{k+1} = R_{1,3}(\tau\mathcal{A})\mathbf{v}^k + \phi_1(\tau\mathcal{A})\mathcal{B}\mathbf{v}^k + \phi_2(\tau\mathcal{A})\mathcal{B}(\mathbf{a}^k + \mathbf{b}^k) + \phi_3(\tau\mathcal{A})\mathcal{B}\mathbf{c}^k, \quad (28)$$

where

$$\begin{aligned} \mathbf{a}^k &= (R_{1,3}(\tau/2\mathcal{A}) + \phi(\tau/2\mathcal{A})\mathcal{B})\mathbf{v}^k \\ \mathbf{b}^k &= R_{1,3}(\tau/2\mathcal{A})\mathbf{v}^k + \phi(\tau/2\mathcal{A})\mathcal{B}\mathbf{a}^k \\ \mathbf{c}^k &= R_{1,3}(\tau/2\mathcal{A})\mathbf{v}^k + \phi(\tau/2\mathcal{A})\mathcal{B}(2\mathbf{b}^k - \mathbf{v}^k), \end{aligned}$$

for  $k = 0, \dots, M - 1$ . By using Taylor expansion, the scheme (28) becomes

$$\begin{aligned} \mathbf{v}^{k+1} &= (1 + (-\mathcal{A} + \mathcal{B})\tau + (\mathcal{A}^2 - 2\mathcal{A}\mathcal{B} + \mathcal{B})\tau^2/2 + (-\mathcal{A}^3 + 3\mathcal{A}^2\mathcal{B} - 3\mathcal{A}\mathcal{B}^2 + \mathcal{B}^3)\tau^3/6 + \\ &\quad (\mathcal{A}^4 - 4\mathcal{A}^3\mathcal{B} + 6\mathcal{A}^2\mathcal{B}^2 - 4\mathcal{A}\mathcal{B}^3 + \mathcal{B}^4)\tau^4/24 + \dots)\mathbf{v}^k. \end{aligned} \quad (29)$$

For  $k = 0, \dots, M - 1$ , the exact solution of system (27) is

$$\mathbf{v}(t_{k+1}) = e^{(-\mathcal{A} + \mathcal{B})\tau}\mathbf{v}(t_k).$$

Therefore, the local truncation error of ETD RK4-P13 method (26) is

$$\begin{aligned} &(1 + (-\mathcal{A} + \mathcal{B})\tau + (\mathcal{A}^2 - 2\mathcal{A}\mathcal{B} + \mathcal{B})\tau^2/2 + (-\mathcal{A}^3 + 3\mathcal{A}^2\mathcal{B} - 3\mathcal{A}\mathcal{B}^2 + \mathcal{B}^3)\tau^3/6 + \\ &\quad (\mathcal{A}^4 - 4\mathcal{A}^3\mathcal{B} + 6\mathcal{A}^2\mathcal{B}^2 - 4\mathcal{A}\mathcal{B}^3 + \mathcal{B}^4)\tau^4/24 + \dots)\mathbf{v}^k - e^{(-\mathcal{A} + \mathcal{B})\tau}\mathbf{v}(t_k) = \mathcal{O}(\tau^5)\mathbf{v}^k. \end{aligned} \quad (30)$$

Hence ETD RK4-P13 method (26) is fourth-order in time discretization.

#### 4.2.2 Stability region of ETDRK4-P13

We demonstrate the linear stability of ETDRK4-P13 method (26) by plotting its stability region. We consider the following nonlinear autonomous ODE

$$u_t + cu = f(u). \quad (31)$$

Linearizing the above equation about a fixed point  $g$  such that  $f(g) - cg = 0$ , we obtain the following test equation

$$u_t + cu = \gamma u, \quad (32)$$

where  $u$  is a perturbation of  $g$  and  $\gamma = f'(g)$ . For all  $\gamma$ , the fixed point  $g$  is stable if  $\text{Re}(\gamma - c) < 0$ .

Applying the semi-discrete ETDRK4-P13 method (26) to the scalar test equation (32) with  $y = -c\tau$  and  $x = \gamma\tau$ , we have the following amplification factor

$$r(x, y) := \frac{u^{k+1}}{u^k} = c_0 + c_1x + c_2x^2 + c_3x^3 + c_4x^4, \quad (33)$$

where

$$\begin{aligned} c_0 &= \frac{6(4+y)}{24-18y+6y^2-y^3}, \\ c_1 &= \frac{169869312 - 148635648y - 9621504y^3 + 470016y^4 + 165888y^5 - 46464y^6 + 6240y^7 - 600y^8 + 32y^9 - y^{10}}{(192-72y+12y^2-y^3)^3(24-18y+6y^2-y^3)}, \\ c_2 &= \frac{442368 - 221184y + 34560y^2 + 11712y^3 - 2976y^4 + 404y^5 - 25y^6 + y^7}{(192-72y+12y^2-y^3)^2(24-18y+6y^2-y^3)}, \\ c_3 &= \frac{2(96-12y+y^2)^2(1536-960y+240y^2+8y^3+y^4)}{(192-72y+12y^2-y^3)^3(24-18y+6y^2-y^3)}, \\ c_4 &= \frac{2(96-12y+y^2)^3(4-3y+y^2)}{(192-72y+12y^2-y^3)^3(24-18y+6y^2-y^3)}. \end{aligned}$$

The stability region is four-dimensional and therefore difficult to visualize. To obtain a two-dimensional stability region, we assume  $c$  to be fixed and real and  $\gamma$  is complex. The boundaries of the stability regions of the ETDRK4-P13 method are obtained by substituting  $r = e^{i\theta}$ ,  $\theta \in [0, 2\pi]$  into (33) and solving for  $x$ . In Fig. 2, we plot the curves of  $|r(x, y)| = 1$  for a complex value of  $x$  and various negative values of  $y$ . According to Beylkin et al. [3], the stability regions should grow as  $y$  approach to  $-\infty$  for the scheme to be useful and practicable. Clearly, the stability regions for the ETDRK4-P13 method as shown in Fig. 2 grow larger as  $y \rightarrow -\infty$  which affirm the stability of the scheme.

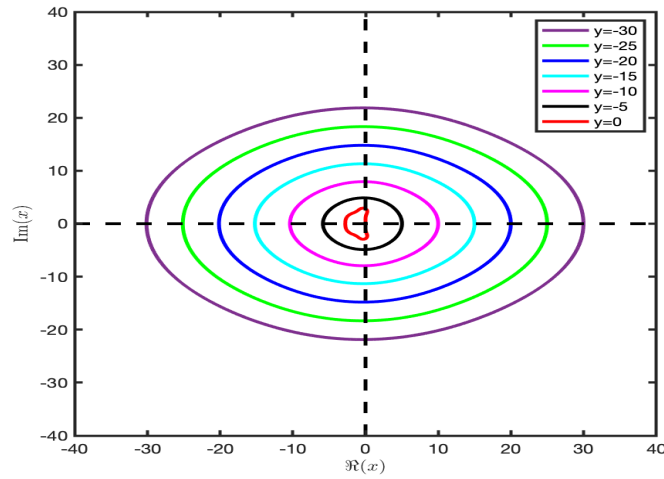


Figure 2: Stability regions of ETDRK4-P13 method in the complex  $x$ -plane.

**Remark 2** *It can be observed from formula (33) that if  $y = 0$ , the amplification factor becomes*

$$r(x, 0) = 1 + x + \frac{1}{2}x^2 + \frac{1}{6}x^3 + \frac{1}{24}x^4,$$

*and it represents the amplification factor of the fourth-order explicit Runge-Kutta (RK4) scheme.*

## 5 Numerical experiments

This section discusses the results obtained by applying the proposed method to various widely known SFRDEs including 2D FitzHugh-Nagumo, Gierer-Meinhardt, Gray-Scott and 3D Schnakenberg models. The accuracy of the scheme is measured in terms of maximum error norm  $\|\cdot\|_\infty$  defined as

$$\|u - u_{h,\tau}\|_\infty = \max_n |u(\mathbf{x}_n, T) - u_n^M|$$

where  $u(\mathbf{x}_n, T)$  and  $u_n^M$  are the  $n$ th exact and numerical solution at the final time  $T$ , respectively. In addition, the order of convergence in space and time is computed as

$$Order = \log_2(E_{h,\tau}/E_{h/2,\tau/2}),$$

where  $E_{h,\tau} = \|u - u_{h,\tau}\|_\infty$  and  $E_{h/2,\tau/2} = \|u - u_{h/2,\tau/2}\|_\infty$  with spatial step size  $h$  and temporal size  $\tau$ . The numerical experiments are performed in MATLAB R2019b platform on a MacBook Pro with 3.1 GHz Dual-Core Intel Core i7 CPU and 8 GB memory.

### 5.1 Stability, accuracy and efficiency tests

The following examples are considered as a benchmark problems in order to investigate the performance in terms of accuracy and efficiency of the proposed method.

**Example 1.** In this example, we consider the following 1D space-fractional Fisher's equation with source term over a domain  $\Omega = [0, 1]$

$$\frac{\partial u}{\partial t} = -\kappa(-\Delta)^{\alpha/2}u + f(u, t), \tag{34}$$

where

$$f(u, t) = -2e^{-t} \sin^3(2\pi x) + \frac{\kappa}{4}e^{-t} (3(2\pi)^\alpha \sin(2\pi x) - (6\pi)^\alpha \sin(6\pi x)) + e^{-2t} \sin^6(2\pi x) + u - u^2,$$

subject to homogenous Dirichlet boundary conditions and the following initial condition

$$g(x) = \sin^3(2\pi x), \quad 0 \leq x \leq 1.$$

The exact solution to (34) is

$$u(x, t) = e^{-t} \sin^3(2\pi x).$$

In the first set of experiments, we compared the analytical solution with solution obtained by the proposed method in order to see how the proposed method is able to capture the spatio temporal solution profile of the component  $u$ . Fig. 3 displays the approximate solution obtained via the proposed method up to  $T = 2$  and the corresponding exact solution for  $\alpha = 2$  and  $\alpha = 1.4$  with  $\kappa = 10$ ,  $N = 64$  and  $\tau = 0.004$ . It is clear from the Fig. 3 that the numerical solution provided by the proposed method is in good agreement with an exact solution.

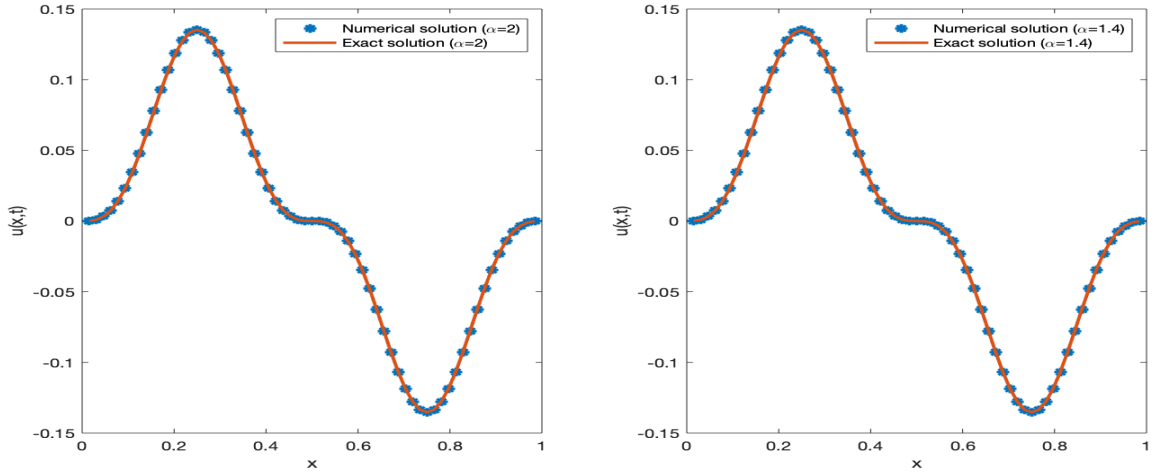


Figure 3: Numerical solutions of Example 1 vs. the exact solution.

In order to do the empirical convergence of the proposed method, we ran a another set of experiments on Example 1 at  $T = 1$  and captured the maximum errors for various values of  $\alpha$ ,  $h$  and  $k$  with  $\kappa = 1$ . In order to visualize the temporal and space rates of convergence of the proposed method, we depicted them in Fig. 4 with log-log scale graph. One can notice that the computed rates of convergences agree with expected order of convergence of the scheme which is a fourth-order accurate in both space and time.

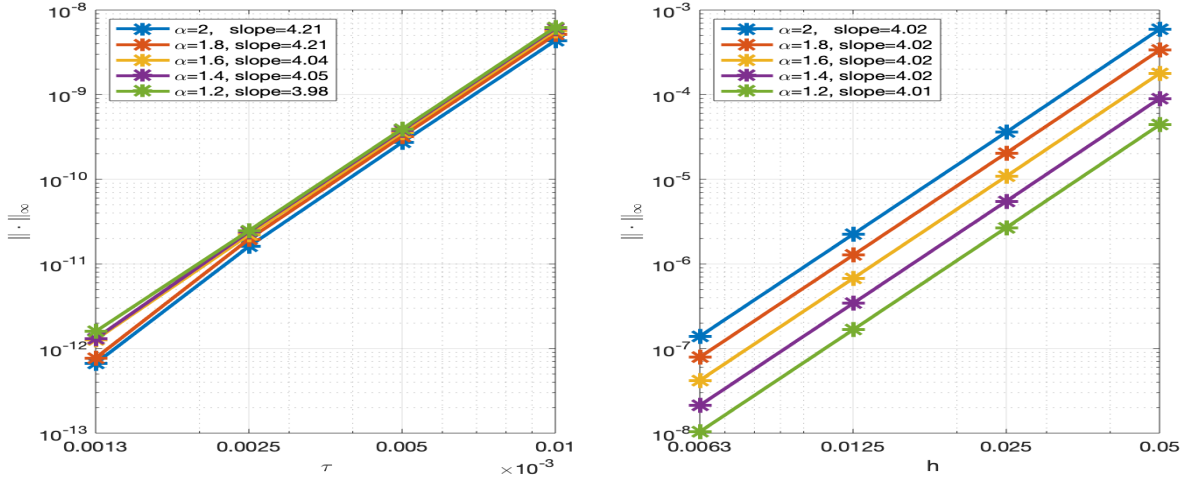


Figure 4: Left label: The log-log graph of errors vs. temporal step size  $\tau$  with  $N = 3000$  and  $\kappa = 1e - 3$ . Right label: The log-log graph of errors vs. spatial step size  $h$  with  $M = 1000$  and  $\kappa = 1e - 3$ .

A third set of experiments ran on Example 1 in order to compare the performance of the proposed method in terms of accuracy and efficiency with the results obtained via the RK4 method for  $\alpha = 1.8$  and different values of  $h$  and  $\tau$ . Maximum errors, rates of convergence, and CPU times for the methods are reported in Table 1. From Table 1, one can see that the temporal step size must be proportional to  $\alpha$  power of the spatial step size  $h$  as expected when the explicit RK4 is used due to the stability constraint from the fractional diffusion term. From Table 1, one can see that the computational cost for the RK4 method is much higher than the proposed method at the same spatial step size  $h$  with similar size of errors and order of accuracy. So, the results in Table 1 justify well enough abandoning the implementation of the RK4 method in the remaining part of this work.

Table 1: Comparison of accuracy and efficiency of the ETD RK4-P13 and RK4 methods for Example 1 34 with  $\kappa = 10$ .

$h$	ETDRK4-P13 $\alpha = 1.8, \tau = \frac{h}{4\kappa}$			RK4 $\alpha = 1.8, \tau = \frac{h}{4\kappa}$			RK4 $\alpha = 1.8, \tau = \frac{h^\alpha}{4\kappa}$		
	$\ \cdot\ _\infty$	Order	CPU(s)	$\ \cdot\ _\infty$	Order	CPU(s)	$\ \cdot\ _\infty$	Order	CPU(s)
$\frac{1}{8}$	1.3871e-02	-	0.0404	NaN	-	0.0332	1.3865e-02	-	0.2278
$\frac{1}{16}$	7.2947e-04	4.25	0.0617	NaN	-	0.0757	7.5050e-04	4.21	0.6722
$\frac{1}{32}$	4.3772e-05	4.06	0.1440	NaN	-	0.1712	4.3772e-05	4.10	2.7245
$\frac{1}{64}$	2.7084e-06	4.01	0.3625	NaN	-	0.4089	2.9474e-06	3.89	11.7495

**Example 2.** Consider the following 2D space-fractional Huxley equation with source term over a domain  $\Omega = [0, 1]^2$

$$\frac{\partial u(x, y, t)}{\partial t} = -\kappa(-\Delta)^{\alpha/2}u + u(1-u)(u-1) + f(x, y, t), \quad (35)$$

where

$$f(x, y, t) = \alpha t^{\alpha-1} \cos^3(2\pi x) \cos^3(2\pi y) + t^\alpha \Phi(x, y) - t^\alpha \cos^3(2\pi x) \cos^3(2\pi y) (1 - t^\alpha \cos^3(2\pi x) \cos^3(2\pi y)) \\ \times (t^\alpha \cos^3(2\pi x) \cos^3(2\pi y) - 1),$$

with

$$\Phi(x, y) = \frac{\kappa}{16} \left( 9(8\pi^2)^{\alpha/2} \cos(2\pi x) \cos(2\pi y) + 3(40\pi^2)^{\alpha/2} \cos(6\pi x) \cos(2\pi y) + 3(40\pi)^{\alpha/2} \cos(2\pi x) \cos(6\pi y) \right. \\ \left. + (72\pi^2)^{\alpha/2} \cos(6\pi x) \cos(6\pi y) \right),$$

subject to periodic and homogenous Neumann boundary conditions. The initial condition can be obtained from the analytical solution  $u(x, y, t) = t^\alpha \cos^3(2\pi x) \cos^3(2\pi y)$ .

To investigate the order of accuracy of the method for varying fractional order  $\alpha$ , a numerical test on Example 2 was performed. In the computation, a simulation was run up to the final time  $T = 1$  with  $\kappa = 1$  by initially setting  $h = 0.1$  and  $\tau = 0.1h$  then reduced both of them by a factor of 2 in each refinement. The maximum error and rates of convergence for  $\alpha = 1.2, 1.4, 1.8, 2.0$  of the diffusion process are listed in Table 2. As expected we observe from Table 2 that the computed convergence rates of the proposed method apparently demonstrate the expected fourth-order accuracy in both time and space for varying  $\alpha$ .

Table 2: Numerical errors, convergence rates and the CPU times for Example 2 with homogenous Neumann or periodic boundary conditions ( $\tau = 0.1h$ ).

$\alpha$	$1/h$	Neumann boundary condition			Periodic boundary condition		
		$\ \cdot\ _\infty$	Order	CPU(s)	$\ \cdot\ _\infty$	Order	CPU(s)
2.0	10	2.5214e-02	-	0.0564	2.5214e-02	-	0.0317
	20	1.4159e-03	4.15	0.2209	1.4159e-03	4.15	0.1897
	40	8.6173e-05	4.04	1.2567	8.6173e-05	4.04	1.0425
	80	5.3493e-06	4.01	8.5284	5.3493e-06	4.01	7.6987
	160	3.3373e-07	4.00	66.3996	3.3373e-07	4.00	58.2910
1.8	10	2.2581e-02	-	0.0583	2.2581e-02	-	0.0307
	20	1.2724e-03	4.15	0.1989	1.2724e-03	4.15	0.1779
	40	7.7475e-05	4.04	1.2673	7.7475e-05	4.04	0.9911
	80	4.8107e-06	4.01	8.4887	4.8107e-06	4.01	7.7161
	160	3.0017e-07	4.00	66.3678	3.0017e-07	4.00	58.1880
1.4	10	1.7272e-02	-	0.0498	1.7272e-02	-	0.0376
	20	9.8009e-04	4.14	0.2529	9.8009e-04	4.14	0.1348
	40	5.9702e-05	4.04	1.2352	5.9702e-05	4.04	0.9927
	80	3.7069e-06	4.01	8.5357	3.7069e-06	4.01	7.7176
	160	2.3115e-07	4.00	68.6389	2.3115e-07	4.00	59.5034
1.2	10	1.4604e-02	-	0.0497	1.4604e-02	-	0.0304
	20	8.3194e-04	4.13	0.2907	8.3194e-04	4.13	0.1361
	40	5.0661e-05	4.04	1.2462	5.0661e-05	4.04	0.9914
	80	3.1332e-06	4.02	8.5007	3.1332e-06	4.02	7.7329
	160	1.9001e-07	4.04	67.0404	1.9001e-07	4.04	58.6672

## 5.2 Some applications

### 5.2.1 2D Fitzhugh-Nagumo model:

The study of the excitable media is made possible using FitzHugh-Nagumo (FHN) model. A cubic nonlinear reaction term is used to model the propagation of the transmembrane potential in the nerve axon [11, 22]

$$\begin{aligned}\frac{\partial u}{\partial t} &= -\kappa(-\Delta)^{\alpha/2}u + u(1-u)(u-\mu) - v, \\ \frac{\partial v}{\partial t} &= \epsilon(\beta u - \gamma v - \delta).\end{aligned}\tag{36}$$

The interest domain is  $\Omega = [0, 2.5]^2$  and the initial conditions are taken as

$$\begin{aligned}u(x, y, 0) &= \begin{cases} 1, & 0 < x \leq 0.125, 0 < y < 0.125, \\ 0, & \text{elsewhere,} \end{cases} \\ v(x, y, 0) &= \begin{cases} 0.1, & 0 < x < 2.5, 0.125 \leq y < 2.5, \\ 0, & 0 < x < 2.5, 0 < y < 0.125. \end{cases}\end{aligned}$$

The choice of parameters  $\mu = 0.1$ ,  $\epsilon = 0.01$ ,  $\beta = 0.5$ ,  $\gamma = 1$  and  $\delta = 0$  is known to generate stable patterns in the system in the form of spiral waves.

In order to illustrate the effect of varying  $\alpha$  and  $\kappa$ , the model is considered subject to periodic [31] or homogenous Neumann boundary conditions [6] with  $N = 256$  and  $\tau = 1$ .

The aerial views of the concentration profile of the component  $v$  subject to periodic boundary conditions with  $\kappa = 1e-4$  at different times and various  $\alpha$  values are presented in Fig. 5 to illustrate the effect of fractional diffusion in FHN model. From Fig. 5, it can be clearly depicted that the width of the wavefront is reduced for decreasing fractional power  $\alpha$ .

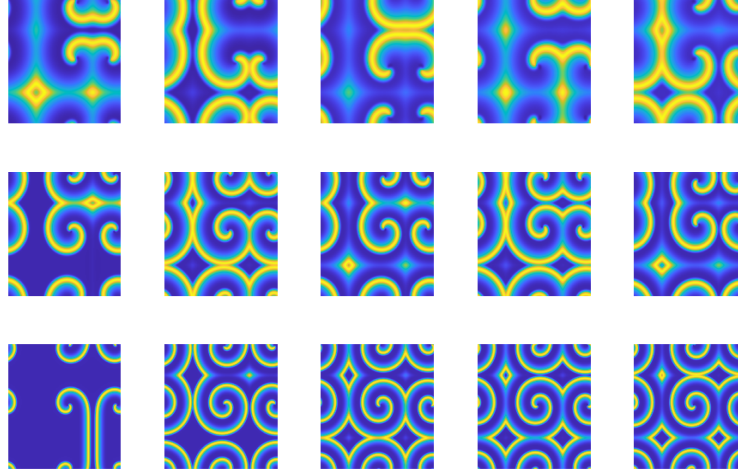


Figure 5: Evolution of the solution  $v$  with  $\kappa = 1e - 4$  for varying  $\alpha = 2, 1.7, 1.5$  (Up-Down) at different time  $T = 400, 700, 1000, 1500, 2000$  (Left-Right).

In the second set of numerical experiments, a stable rotating solution of the component  $v$  at  $T = 2000$  is also presented in Fig. 6 to illustrate the effect fractional diffusion and diffusion coefficient in the model subject to homogenous Neumann boundary conditions with  $\kappa = 1e - 4$  and varying  $\alpha$ . It can be clearly seen from Fig. 6 that the role of reducing the fractional power  $\alpha$  is not equivalent to the influence of a decreased diffusion coefficient in the pure diffusion case (Fig. 7).

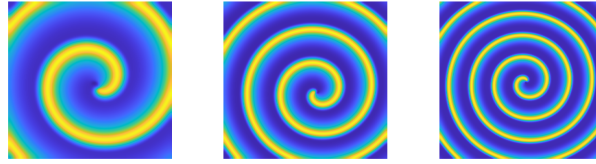


Figure 6: Spiral waves for varying  $\alpha = 2, 1.7, 1.5$  (Left-Right) and  $\kappa = 1e - 4$  at  $T = 2000$ .

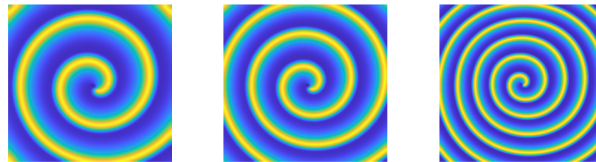


Figure 7: Spiral waves for  $\alpha = 2$  and varying diffusion coefficient  $\kappa = 5e - 5, 3e - 5, 1e - 5$  (Left-Right) at  $T = 2000$ .

### 5.2.2 2D Gierer-Meinhardt model:

The Gierer–Meinhardt model is widely used in the study of some basic phenomena in the process of morphogenesis. Here, we consider the following fractional Gierer–Meinhardt model [12]:

$$\begin{aligned} \frac{\partial u}{\partial t} &= -\kappa_u (-\Delta)^{\alpha/2} u + \frac{u^2}{v} - u \\ \frac{\partial v}{\partial t} &= -\kappa_v (-\Delta)^{\beta/2} v + \frac{u^2}{\epsilon \mu} - \frac{v}{\mu}, \end{aligned} \tag{37}$$

on  $\Omega = [-1, 1]^2$  with homogenous Neumann boundary condition. The parameters are chosen as  $\epsilon = 0.04$ ,  $\mu = 0.1$ . The diffusion coefficient are taken as  $\kappa_u = \epsilon^2$  and  $\kappa_v = \frac{K}{\mu}$ . The initial condition are chosen as

$$u(x, y, 0) = \frac{1}{2} \left( 1 + 0.001 \sum_{j=1}^{20} \cos\left(\frac{\pi}{2} j y\right) \right) \text{sech}^2 \left( \frac{\sqrt{x^2 + y^2}}{2\epsilon} \right),$$

$$v(x, y, 0) = \frac{\cosh(1 - \sqrt{x^2 + y^2})}{3 \cosh(1)}.$$

In this set of numerical experiments, we chose  $N = 64$ ,  $\tau = 0.1$  and  $K = 0.0162$  and ran the simulation profile of the component  $u$  for fixed  $\alpha = 2$  and different values of  $\beta$  at different times  $T$  and depicted in Fig. 8. As shown in [28], Turing instability will appear for  $\beta < 1.8$ , so the results were omitted here. In Fig. 8, it can be observed that the stripe pattern for  $\beta = 1.8$ . If we keep increasing the value of  $\beta$ , then a chain cluster of Turing spotted patterns initially evolve. The pure Turing spot patterns are clearly obtained when the simulation time increases to 1000; as seen in Fig. 8. In Fig. 9, we plot the solution of  $u$  for different  $\alpha$  and  $\beta$  at different times  $T$ . Again, a chain cluster of Turing spotted patterns appear as time increases.

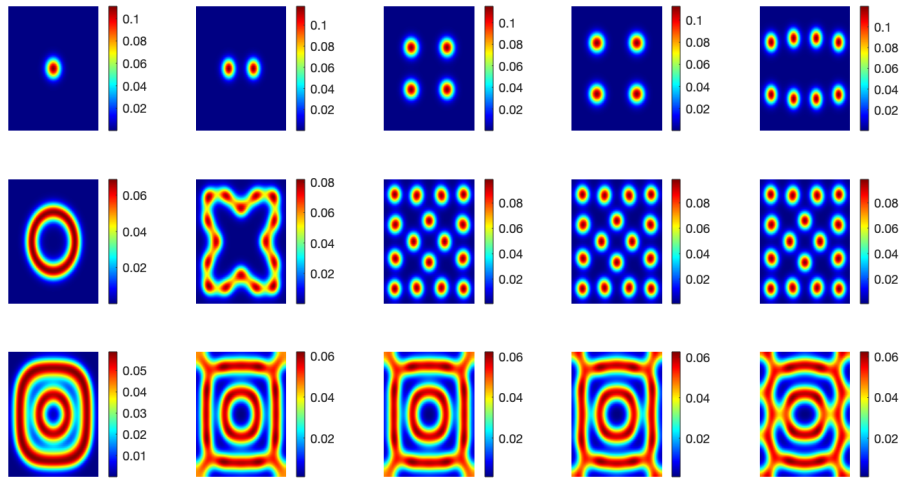


Figure 8: Turing pattern in the Gierer-Meinhardt model (37) for  $K = 0.0162$ ,  $\alpha = 2$  and varying  $\beta = 2, 1.9, 1.8$  (Up-Down) at  $T = 100, 300, 500, 700, 1000$  (Left-Right).



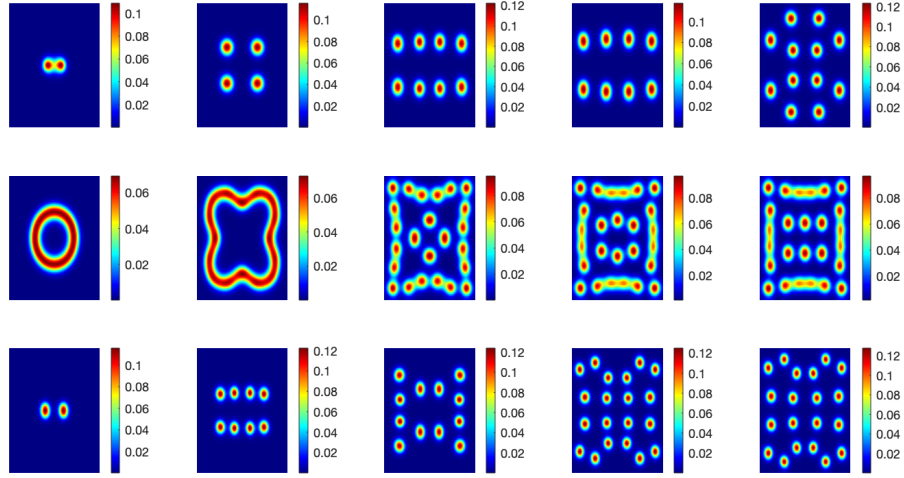


Figure 9: Turing pattern in the Gierer-Meinhardt model (37) for  $K = 0.0162$  and varying  $(\alpha, \beta) = (1.9, 1.9), (1.9, 1.8), (1.8, 1.8)$  (Up-Down) at  $T = 100, 300, 500, 700, 1000$  (Left-Right).

In the second set of numerical experiments, we consider the case for  $K = 0.0128$ . Figs. 10 and 11 exhibit the scenarios of pattern formation for different values of  $\alpha$  and  $\beta$  at different times  $T$ . In Fig. 10, we fix  $\alpha = 2$  and vary  $\beta$ . When  $\beta = 1.8$ , then the system become stable, that is, the solution approaches the steady state  $\epsilon = 0.04$  while Turing patterns appear when  $\beta$  increases, as seen in Fig. 10. In Fig. 11, one can observe that a stripe pattern turns into a spot pattern for different  $\alpha$  and  $\beta$ . For more details, we refer to [28, 10, 24, 21].

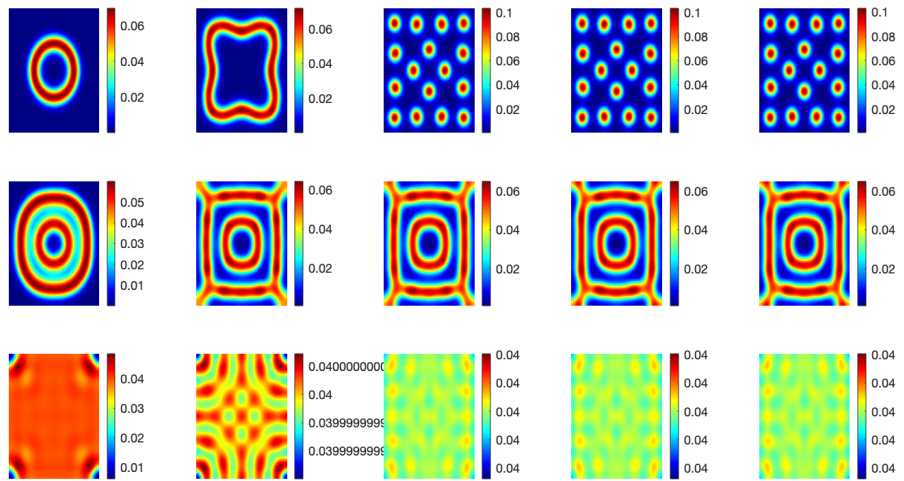


Figure 10: Turing pattern in the Gierer-Meinhardt model (37) for  $K = 0.0128$ ,  $\alpha = 2$  and varying  $\beta = 2, 1.9, 1.8$  (Up-Down) at  $T = 100, 300, 500, 700, 1000$  (Left-Right).

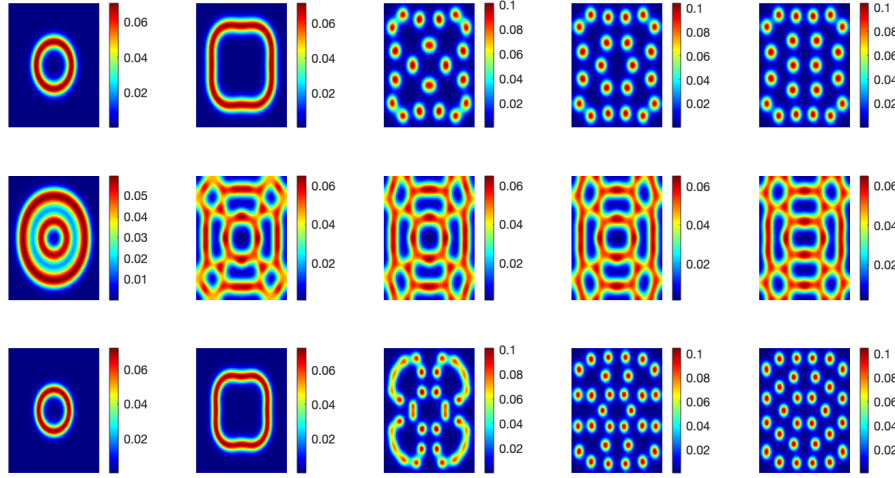


Figure 11: Turing pattern in the Gierer-Meinhardt model (37) for  $K = 0.0128$  and varying  $(\alpha, \beta) = (1.9, 1.9), (1.9, 1.8), (1.8, 1.8)$  (Up-Down) at  $T = 100, 300, 500, 700, 1000$  (Left-Right).

### 5.2.3 2D Gray-Scott model:

The fractional Gray-Scott model that describes an autocatalytic reaction-diffusion process between two chemical species with concentrations  $u$  and  $v$  is written as [13, 14]

$$\begin{aligned} \frac{\partial u}{\partial t} &= -\kappa_u (-\Delta)^{\alpha/2} u - uv^2 + F(1 - u), \\ \frac{\partial v}{\partial t} &= -\kappa_v (-\Delta)^{\alpha/2} v + uv^2 - (F + K)v, \end{aligned} \quad (38)$$

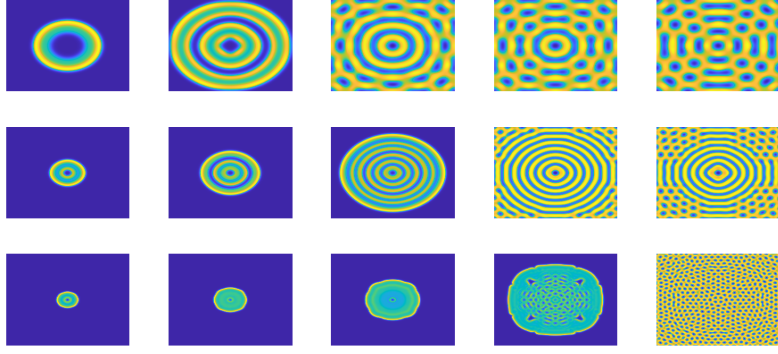
The diffusion rates in the process satisfy  $\kappa_u \geq 0, \kappa_v \geq 0$ . The parameters  $F, K$  are the dimensionless feed rate and decay rate, respectively. The spatially initial condition is

$$(u, v) = \begin{cases} (1, 0), & (x, y) \in \Omega \setminus O, \\ (\frac{1}{2}, \frac{1}{4}), & (x, y) \in O, \end{cases}$$

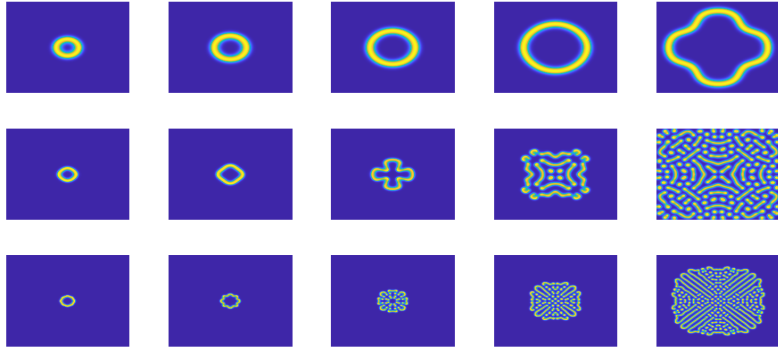
where  $\Omega = (0, 1)^2$  and  $O = \{(x, y) | (x - 0.5)^2 + (y - 0.5)^2 \leq 0.0016\}$ . We take  $N = 265, \tau = 1, F = 0.03$  and varying  $K, \alpha$ . The ratio of diffusion coefficients are chosen as  $\kappa_u = 2e - 5, \kappa_v = 1e - 5$  ( $\kappa_u/\kappa_v > 1$ ) to make the model generating different types of pattern formation [29].

The evolution profile of the component  $v$  and the effects of the super-diffusion for the fractional Gray-Scott model are shown in Fig. 12. From the Fig. 12, it can be seen that the speeds of pattern formulation depend on different  $\alpha$  due to the speed of the diffusion is affected by fractional order.

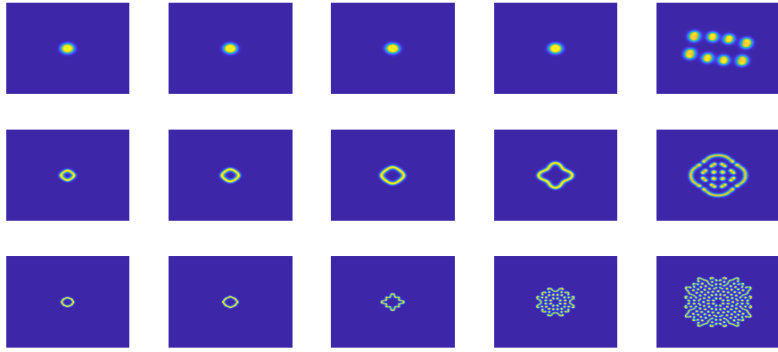
For  $K = 0.055$  (Fig. 12a), the model with the normal diffusion ( $\alpha = 2$ ) produce a circular wave propagating outward. Moreover, the reduction of the fractional order  $\alpha = 1.7$  affects the size of patterns with smaller spots and generates a decrease in the velocity of the propagation of the initial perturbation. For smaller values of the fractional power ( $\alpha = 1.5$ ), we observe a new process of pattern formation. The process of nucleation of the structure propagates outward until the entire domain reaches the final steady state. For  $K = 0.061$  (Fig. 12b), the model presents filaments and produces a wavefront propagation by curvature. When the order  $\alpha$  of the fractional Laplacian operator decreases, the curvature driven mechanisms are increased and filaments become thinner. For  $K = 0.063$  (Fig. 12c), the model exhibits patterns of the mitosis when  $\alpha = 2$ . However, when the fractional order of the model is decreased, the replication pattern is completely changed as shown in Fig. 12c.



(a)  $K = 0.055$ ,  $\alpha = 2, 1.7, 1.5$  (Up-Down),  $T = 500, 1000, 2000, 4000, 8000$  (Left-Right).



(b)  $K = 0.061$ ,  $\alpha = 2, 1.7, 1.5$  (Up-Down),  $T = 500, 1000, 2000, 4000, 8000$  (Left-Right).



(c)  $K = 0.063$ ,  $\alpha = 2, 1.7, 1.5$  (Up-Down),  $T = 500, 1000, 2000, 4000, 8000$  (Left-Right).

Figure 12: Pattern formation in the Gray-Scott model (38) for different values of parameter  $K$  and fractional power  $\alpha$ .

#### 5.2.4 3D Schnakenberg model

We consider the system of 3D space-fractional Schnakenberg model [15]:

$$\begin{aligned} \frac{\partial u}{\partial t} &= -\kappa_u(-\Delta)^{\alpha/2}u + \gamma(a - u + u^2v), \\ \frac{\partial v}{\partial t} &= -\kappa_v(-\Delta)^{\alpha/2}v + \gamma(b - u^2v). \end{aligned} \tag{39}$$

Subject to periodic boundary conditions and initial condition:

$$\begin{aligned} u(x, y, z, 0) &= 1 - e^{-10((x-l/2)^2 + (y-l/2)^2 + (z-l/2)^2)}, \\ v(x, y, z, 0) &= e^{-10((x-l/2)^2 + 2(y-l/2)^2 + (z-l/2)^2)}, \end{aligned}$$

where  $u$  and  $v$  are the concentration of the chemical products,  $\kappa_u, \kappa_v$  are the diffusion coefficients,  $\gamma$  is the scale factor proportional to the length of the domain,  $a, b$  are the positive constants, and  $l$  is the length of domain. The parameters are selected as follows:  $\kappa_u = 1, \kappa_v = 10, \gamma = 1, a = 0.1, b = 0.9$ . We simulate the model on the domain  $\Omega = (0, l)^3$  with  $N = 32$  and  $\tau = 1$ .

Numerical simulation of the Schnakenberg model in three spatial dimensions represents an even more amazing scenario where more exotic and chaotic patterns may arise which illustrate the emergence of pattern formation dependent on the values of  $T$ , the length of the domain and the fractional power  $\alpha$ , as can be observed in Figs. 13, 14 and 15.

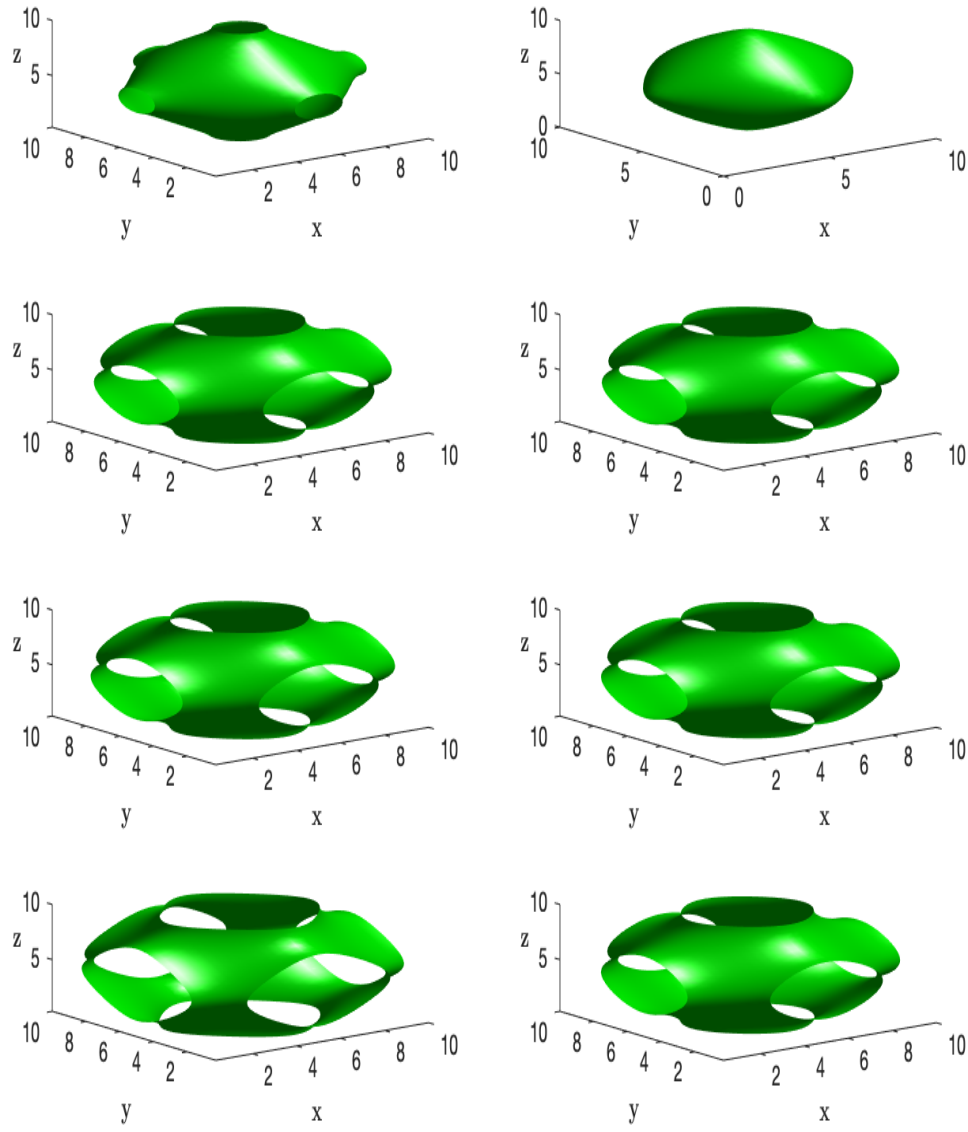


Figure 13: Snapshots of the evolution of substrate  $v$  for 3D Schnakenberg model (39) with  $l = 10$  and  $\alpha = 2, 1.5$  (Left-Right) at  $T = 5, 20, 100, 200$  (Up-Down).

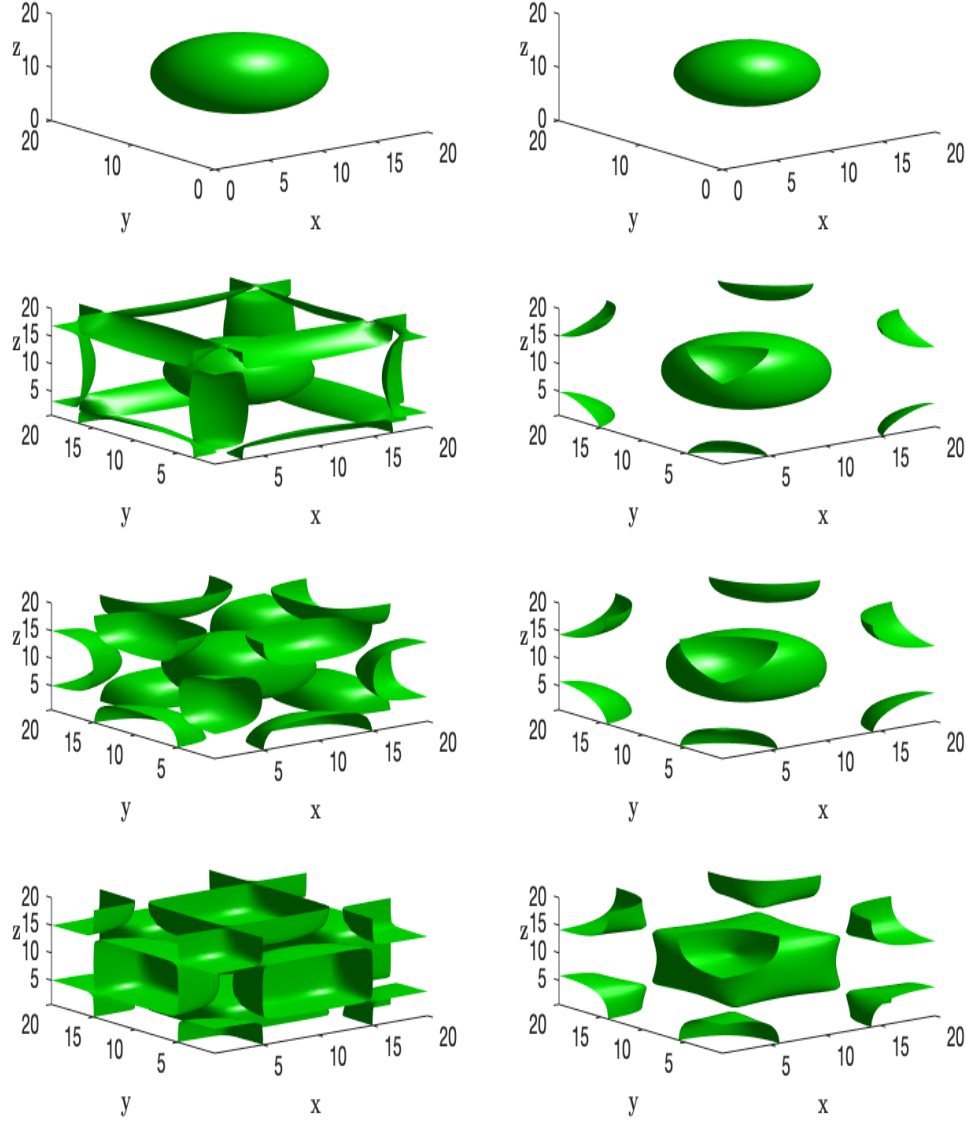


Figure 14: Snapshots of the evolution of substrate  $v$  for 3D Schnakenberg model (39) with  $l = 20$  and  $\alpha = 2, 1.5$  (Left-Right) at  $T = 5, 20, 100, 200$  (Up-Down).

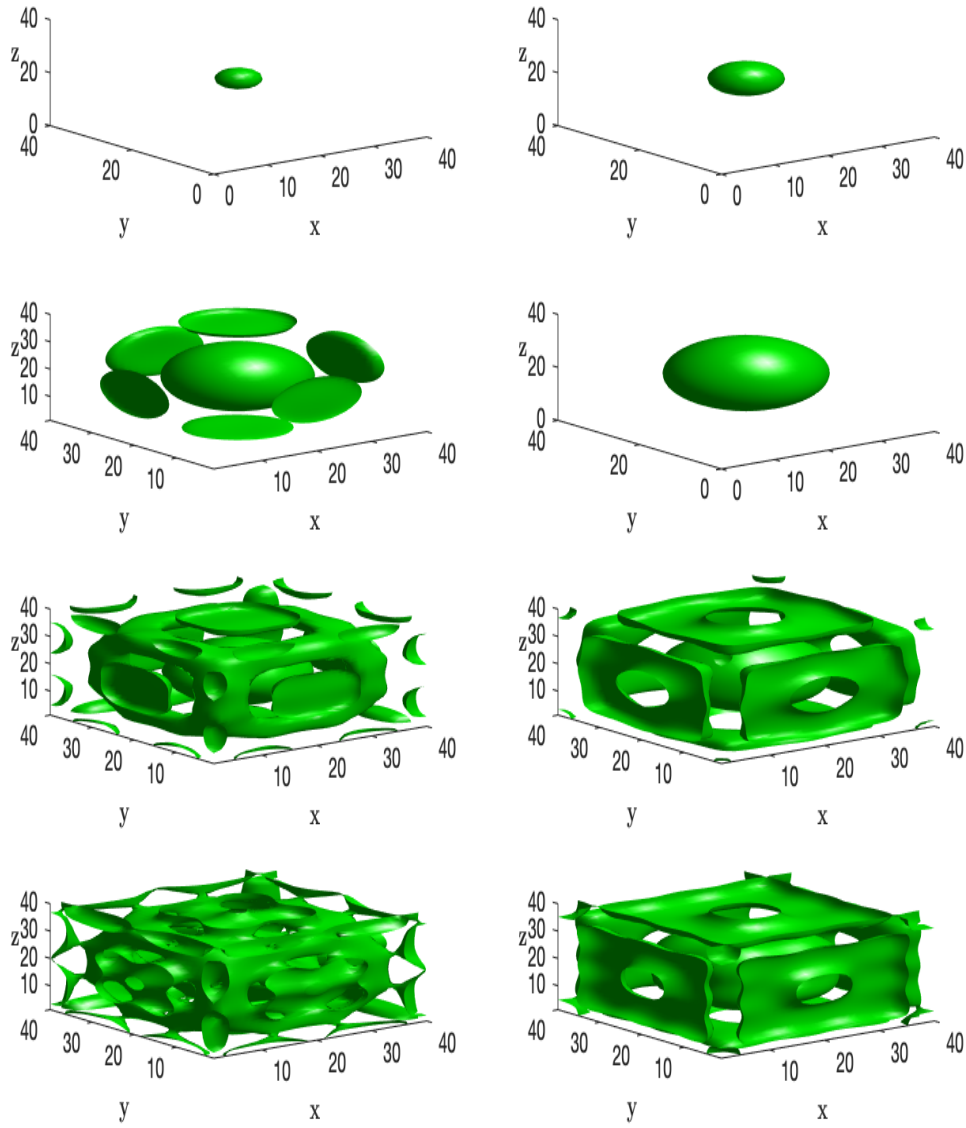


Figure 15: Snapshots of the evolution of substrate  $v$  for 3D Schnakenberg model (39) with  $l = 40$  and  $\alpha = 2, 1.5$  (Left-Right) at  $T = 5, 20, 100, 200$  (Up-Down).

## 6 Conclusion

In this manuscript, a fast, accurate, and stable high-order numerical method is proposed for solving space-fractional reaction-diffusion equations with subject to periodic, Dirichlet or Neumann boundary conditions. The proposed method is based on a fourth-order exponential time differencing Runge-Kutta approximations for time integration and a fourth-order compact finite difference approximation in combination with matrix transfer technique for spatial approximation, that allow use of FFT-based fast calculations. An empirical convergence analysis and calculation of local truncation error exhibited the fourth-order accuracy of the proposed method. The performance (in terms of accuracy

and efficiency) and reliability of the method has been investigated by testing it on various numerical examples including 2D fractional Fitzhugh-Nagumo, Gierer-Meinhardt, Gray-Scott and 3D fractional Schnakenberg models. The numerical results exhibited that the proposed method is fast, accurate and applicable for simulating the multi-dimensional space-fractional reaction-diffusion equations. In future, the method will be applied to multi-dimensional space-fractional reaction-diffusion-advection equations involving non smooth data.

## References

- [1] L. Aceto, P. Novati, Rational approximation to the fractional Laplacian operator in reaction-diffusion problems, *SIAM J. Sci. Comput.* 39 (1) (2017) A214-A228.
- [2] S. S. Alzahrani, A. Q. M. Khaliq, T. A. Biala, K. M. Furati, Fourth-order time stepping methods with matrix transfer technique for space-fractional reaction-diffusion equations, *Appl. Numer. Math.* 146 (2019) 123-144.
- [3] G. Beylkin, J. Keiser, L. Vozovoi, A new class of time discretization schemes for the solution of nonlinear PDEs, *J. Comput. Phys.* 147 (1998) 362-387.
- [4] H. P. Bhatt, A. Q. M. Khaliq, A compact fourth-order L-stable scheme for reaction-diffusion systems with nonsmooth data, *J. Comput. Appl. Math.* 299 (2016) 176-193.
- [5] H. P. Bhatt, A. Q. M. Khaliq, Efficient high-order compact exponential time differencing method for space-fractional reaction-diffusion systems with nonhomogeneous boundary conditions, *Numer. Algor.* (2019) 1-25.
- [6] A. B. Orovio, D. Kay, K. Burrage, Fourier spectral methods for fractional-in-space reaction-diffusion equations, *BIT Numer. Math.* 54 (2014) 937-954.
- [7] P. Constantin, M. Ignatova, Remarks on the fractional Laplacian with Dirichlet boundary conditions and applications, *Int. Math. Res. Notices* 6, (2016) 1653-1673.
- [8] H. fei Ding, Y. xin Zhang, New numerical methods for the Riesz space-fractional partial differential equations, *Comput. Math. Appl.* 63 (7) (2012) 1135-1146.
- [9] S. Duo, H. Wang, Y. Zhang, A comparative study on nonlocal diffusion operators related to the fractional Laplacian, *arXiv preprint arXiv:1711.06916* (2017) 1-25.
- [10] R. Fernandes, G. Fairweather, An ADI extrapolated Crank-Nicolson orthogonal spline collocation method for nonlinear reaction-diffusion systems, *J. Comput. Phys.* 231 (2012) 6248-6267.
- [11] R. FitzHugh, Impulses and physiological states in theoretical models of nerve membrane, *Biophys. J.* 1 (1961) 445.
- [12] A. Gierer, H. Meinhardt, A theory of biological pattern formation, *Kybernetik* 12 (1992) 30-39.
- [13] P. Gray, S. K. Scott, Autocatalytic reactions in the isothermal, continuous stirred tank reactor: isolas and other forms of multistability, *Chem. Eng. Sci.* 38 (1983) 29-43.
- [14] P. Gray, S. K. Scott, Sustained oscillations and other exotic patterns of behavior in isothermal reactions, *J. Phys. Chem.* 89 (1985) 22-32.
- [15] W. R. Holmes, An efficient, nonlinear stability analysis for detecting pattern formation in reaction diffusion systems, *Bull. Math. Biol.* 76 (2014) 157-183.
- [16] J. Huang, L. Ju, B. Wu, A fast compact exponential time differencing method for semilinear parabolic equations with Neumann boundary conditions, *Appl. Math. Lett.* 94 (2019) 257-265.
- [17] J. Huang, L. Ju, B. Wu, A fast compact time integrator method for a family of general order semilinear evolution equations, *J. Comput. Phys.* 393 (2019) 313-336.
- [18] M. Ilic, F. Liu, I. Turner, V. Anh, Numerical approximation of a fractional-in-space diffusion equation I, *Fract. Calc. Appl. Anal.* 8 (2005) 323-341.
- [19] M. Ilic, F. Liu, I. Turner, V. Anh, Numerical approximation of a fractional-in-space diffusion equation (II)-with nonhomogeneous boundary conditions, *Fract. Calc. Appl. Anal.* 9 (2006) 333-349.
- [20] L. Ju, J. Zhang, L. Zhu, Q. Du, Fast explicit integration factor methods for semilinear parabolic equations, *J. Sci. Comput.* 62 (2015) 431-455.
- [21] M. McCourt, N. Dovidio, M. Gilbert, Spectral methods for resolving spike dynamics in the Gierer-Meinhardt model, *Comput. Phys.* 3 (2008) 659-678.
- [22] J. Naqumo, S. Arimoto, S. Yoshizawa, An active pulse transmission line simulating nerve axon, *Proceedings of the IRE* 50 (1962) 2061-2070.



- [23] C. Pozrikidis, The Fractional Laplacian, Chapman and Hall/CRC (2016).
- [24] Z. Qiao, Numerical investigations of the dynamical behaviors and instabilities for the Gierer-Meinhardt system, Commun. Comput. Phys. 3 (2008) 406-426.
- [25] F. Song, C. Xu, G. Em Karniadakis, Computing fractional Laplacians on complex-geometry domains: algorithms and simulations, SIAM J. Sci. Comput. 39 (2017) A1320-A1344.
- [26] I. Turner, M. Ilic, P. Perron, The use of fractional-in-space diffusion equations for describing microscale diffusion in porous media, Dechema (2010).
- [27] C. V. Loan, Computational frameworks for the fast Fourier transform, Frontiers in Applied Mathematics 10 (1992).
- [28] Y. Wang, R. Zhang, Z. Wang, Z. Han, Turing pattern in the fractional Gierer-Meinhardt model, Chinese Phys. B 28 (2019) 050503.
- [29] T. Wang, F. Song, H. Wang, G. Em Karniadakis, Fractional Gray-Scott model: Well-posedness, discretization, and simulations, Comput. Methods in Appl. Mech. Eng 347 (2019) 1030-1049.
- [30] Q. Yang, F. Liu, I. Turner, Numerical methods for fractional partial differential equations with Riesz space-fractional derivatives, Appl. Math. Model. 34, (2010) 200-218.
- [31] H. Zhang, X. Jiang, F. Zeng, G. Em Karniadakis, A stabilized semi-implicit Fourier spectral method for nonlinear space-fractional reaction-diffusion equations, J. Comput. Phys. 405 (2020) 109-141.
- [32] S. Zhao, J. Ovadia, X. Liu, Y. T. Zhang, Q. Nie, Operator splitting implicit integration factor methods for stiff reaction-diffusion-advection systems, J. Comput. Phys. 230 (2011) 5996-6009.
- [33] L. Zhu, L. Ju, W. Zhao, Fast high-order compact exponential time differencing Runge-Kutta methods for second-order semilinear parabolic equations, J. Sci. Comput. 67 (2016) 1043-1065.
- [34] P. Zhuang, F. Liu, V. Anh, I. , Numerical methods for the variable-order fractional advection-diffusion equation with a nonlinear source term, SIAM J. Numer. Anal. 47 (2009) 1760-1781.